Reports

Axial Oxygen–Centered Lattice Instabilities and High-Temperature Superconductivity

STEVEN D. CONRADSON, IAN D. RAISTRICK, ALAN R. BISHOP

Copper K-edge x-ray absorption data indicate that an axial oxygen–centered lattice instability accompanying the 93 K superconducting transition in $YBa_2Cu_3O_7$ is of a pseudo-(anti)ferroelectric type, in that it appears to involve the softening of a double potential well into a structure in which the difference between the two copper-oxygen distances and the barrier height have both decreased. This softer structure is present only at temperatures within a fluctuation region around the transition. A similar process involving the analogous axial oxygen atom also accompanies the superconducting transition in $TlBa_2Ca_3Cu_4O_{11}$, where the superconducting transition temperature T_c is ~120 K. The mean square relative displacement of this oxygen atom in $YBa_2Cu_3O_7$ is also specifically affected by a reduction in the oxygen content and by the substitution of cobalt for copper, providing further evidence for the sensitivity of the displacement to additional factors that also influence the superconductivity. On the basis of the implied coupling of this ionic motion to the superconductivity, a scenario for high-temperature superconductivity is presented in which both phonon and electronic (charge transfer) channels are synergistically involved.

TWO AND ONE-HALF YEARS AFTER the discovery of the new copper oxide–based materials (*1*), consensus on the mechanism of superconductivity in these and related compounds is still lacking (*2*). Phonon-mediated pairing alone seems unreasonable for the materials with high T_c, for example, $YBa_2Cu_3O_7$ ($T_c = 93$ K), $TlBa_2Ca_3Cu_4O_{11}$ ($T_c \sim 120$ K), and other compounds with T_c values significantly higher than 30 to 40 K (*3*). In contrast, other oxides with T_c values ≤ 30 K (*4*) apparently show conventional superconductivity with a large electron-phonon coupling constant (*5*). A distinctive structural unit in the higher temperature systems is an axial O atom that forms a bridge between the supercurrent-carrying CuO_2 planes and an adjacent layer of highly polarizable copper, thallium, or bismuth oxide (Fig. 1) (*6*).

A large body of experimental evidence (*6–8*) supports the idea that the axial O site is indeed involved in the superconductivity of this class of compounds. Recently, additional information has become available that further implicates this structural feature. First, x-ray absorption fine structure (XAFS) spectroscopy has shown that a lattice instability involving the axial O atom accompanies the superconducting transition in $YBa_2Cu_3O_7$ (*9*). Second, heat capacity measurements show anomalies around T_c in $YBa_2Cu_3O_7$ and several Tl- and Bi-based compounds (*10*). The magnitude of the effect seems to be far larger than those easily associated with electron pairing and may therefore reflect an associated structural perturbation. Third, the anomalously large infrared absorption (*11, 12*) and excitation dependence of the Raman features (*13*) of vibrational modes parallel to the *c* axis suggest that such a lattice instability could be coupled to charge transfer, as observed in superconducting intercalated graphite (*14*). Finally, whereas the increase of T_c with pressure for copper oxide–based compounds containing axial O atoms is larger than for conventional superconductors, no pressure-dependent change in T_c occurs for $Nd_{1.85}Ce_{0.15}CuO_{4-\delta}$ (which does not contain these moieties) (*15*).

Discrepancies, particularly in the thermal parameters, in the crystallographic results from different groups (*16*) suggest that diffraction methods are insensitive to some disorder-related structural features. Such difficulties are particularly likely to occur when atoms are involved in strongly anharmonic vibrations (*17*); it is notable that the positions of the axial O atoms tend to be the least certain (*18, 19*). In contrast to diffraction experiments, XAFS is sensitive not to the positions of the atoms within the unit cell but to the atom positions relative to the selected absorbing element (*20, 21*). XAFS may therefore be used to identify subtle, disorder-related changes in the crystal structure that can elude diffraction methods, especially when the use of oriented samples allows the contribution of a particular moiety to be isolated (*21, 22*). We describe here Cu K-edge x-ray absorption measurements on magnetically oriented (*23*) $YBa_2Cu_3O_7$ and derivatives and on unoriented $TlBa_2Ca_3Cu_4O_{11}$, which suggest a more active role for the axial O atom than that found crystallographically and present a framework for a connection between these results and high-temperature superconductivity.

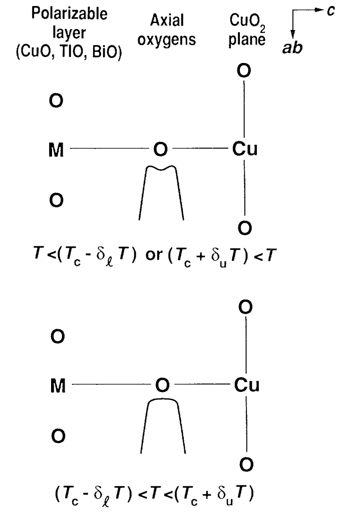

Fig. 1. Generic structure of a high-T_c compound showing the supercurrent-carrying CuO_2 plane, the axial O atom, and the polarizable MO layer [after (*6*)]. The cations of the insulating layer, which are coordinated to the axial O atoms have been omitted for clarity. The suggested types of *c*-oriented O4 radial distribution functions outside of (top) and within (bottom) the fluctuation region are shown underneath that atom.

Samples of $YBa_2Cu_3O_{6.97}$, $YBa_2Cu_3O_{6.51}$, and $YBa_2Cu_{2.8}Co_{0.2}O_{7+\delta}$ were prepared and analyzed by standard procedures. X-ray powder diffraction analysis indicated that all the samples were single-phase. $YBa_2Cu_3O_7$ showed an onset of diamagnetism, T_c, at 93 K; the halfway point of the transition as measured by magnetic field exclusion, $T_{1/2}$, was 82 K in a field of 100 G, with 100% exclusion at 7 K; $YBa_2Cu_{2.8}Co_{0.2}O_{7+\delta}$ had a $T_{1/2}$ of 25 K and 50% exclusion; $YBa_2Cu_3O_{6.51}$ had a $T_{1/2}$ of 52 K and 30% exclusion. We also prepared $TlBa_2Ca_3Cu_4O_{11}$ by standard procedures, using a Tl overpressure before the final O_2 anneal in a MgO tube. X-ray powder diffraction analysis of this material showed that it contained ~85% of the $TlBa_2Ca_3Cu_4O_{11}$ phase [T_c ~120 K (*24*)]. This sample showed a T_c of 118 K, a $T_{1/2}$ of 103 K, and 100% exclusion. We made the oriented samples by mixing the powder with epoxy (*23*), which

---

Electronics Research, Isotope and Structural Chemistry, and Condensed Matter and Statistical Physics Groups, Los Alamos National Laboratory, Los Alamos, NM 87545.

was allowed to set in a field of 4 T. X-ray pole figure analysis showed preferred textures in excess of 90 to 95%. Samples were mounted in an Al holder attached to the cold finger of a liquid He cryostat. The listed temperatures are those of the cold finger, and thus the actual temperature of the samples may be up to 5 to 10 K higher. We recorded all XAFS data at the Stanford Synchrotron Radiation Laboratory (SSRL) on beam lines I-5 and II-2, using Si[220] crystals (detuned 50% with θ, where θ is the orientation of the faces of the two crystals) under dedicated operating conditions (electron energy, 3.0 GeV; stored current, 15 to 50 mA). We minimized Fourier transform artifacts by performing these calculations, as well as the background subtractions, with identical or very similar parameters for spectra from the same sample. To minimize cutoff effects, we performed the filtering over a region 1 Å^{-1} wider on each end than the fitting range.

On the basis of the standard notation for $YBa_2Cu_3O_7$ (*16*), the CuO_2 sheets are composed of the Cu2 and O2,3 atoms, the CuO_3 chains are composed of Cu1 and O1,4, where O4 is the axial O. The contribution of the Cu1–O4 pair dominates the prominent Fourier transform modulus peak, which is located at radius R = 1.5 Å (because of the phase shift) in the electric field parallel to the *c* axis ($\mathbf{E} \parallel c$) data in Fig. 2 (*21*). At high ($T \geq 88$ K) and low ($T \sim 10$ K) temperature, this peak exhibits a shoulder or related asymmetry near 1.8 Å but appears much narrower and more symmetric for $45 \leq T \leq 86$ K. The expected, identical temperature dependence is apparently exhibited by the Cu2–O4 extended x-ray absorption fine structure (EXAFS) spectroscopy; one large peak between 1.9 and 2.4 Å is observed in coincidence with the 1.8 Å shoulder or asymmetry, and two small peaks occur in this region at 45, 82, and 86 K. Some small changes also occur in the Cu1–Cu2 wave between 82 and 95 K, which could originate in the behavior of O4 via multiple scattering effects (*25*) and thus corroborate the Cu–O behavior.

Curve fits based on the use of harmonic Debye-Waller factors (*26*) demonstrate that the average Cu1–O4 distance of ~1.9 Å is invariant. However, the behavior of these fits is strongly indicative of a large anharmonic component in the Cu1–O4 radial distribution function (RDF) (*27*). Direct comparisons of the EXAFS from the Cu1–O4 pair (Fig. 2), obtained by Fourier-filtering, that is, back-transforming from the range in real space where this shell makes its primary contribution, therefore provide the best means for interpreting the EXAFS. The EXAFS are very similar out to $\mathbf{k} \sim 10$ Å^{-1} ($\mathbf{k}$ is a "wave vector" related to momentum) at all temperatures. However, for $T \geq 88$ K or at 10 K the local minimum in the amplitude and the irregularity in the phase near 12 Å^{-1} constitute a "beat," which signifies the presence of at least two waves from shells at different distances. In addition, the very rapid damping of these Cu–O waves relative to the $\mathbf{E} \parallel ab$ data [or to those from La_2CuO_4 and related compounds (*28*)] indicates that the Cu1–O4 mean square relative displacement (MSRD) either is unexpectedly large or contains a significant anharmonic component. If we use the relation Δdistance = $\pi/2\mathbf{k}$ between the separation of two shells and the position of the beat, the Cu–O distances differ by 0.10 to 0.12 Å.

Closer examination of these data reveals the details of the temperature dependence detected in the transforms. When the nominal temperature is lowered from 88 to 105 K to 82 to 86 K, the phase loses its distinct beat and the amplitude decreases very rapidly and monotonically from its peak at $\mathbf{k}$ = 7.5 Å^{-1} to essentially zero at 14 Å^{-1}. These EXAFS are what would be expected if the difference between the two Cu1–O4 distances was now smaller. At ~10 K, the EXAFS has become very similar to that at 105 K, which indicates a corresponding structural similarity. This result is in agreement with the work of Yang *et al.* (*21*), who also found that the Cu1,2–O4 MSRDs were very similar at 10 and 90 K.

The structure suggested by these data (Fig. 1) is an anharmonic double well with two distinct Cu1–O4 positions that are approximately equally populated above T_c. Because both positions are occupied simultaneously, this could be either a degenerate structure with one O atom at each minimum within a unit cell or a cell-doubling structure with alternating long-long and short-short distances at the Cu1 sites. At lower temperatures within a "fluctuation" region close to the superconducting transition ($T_c - \delta_\ell T \lesssim T \lesssim T_c + \delta_u T$), the double well softens, that is, two minima approach each other more closely and the height of the local maximum in the potential surface between the two wells decreases (*29*). As the temperature is lowered further, this process is reversed.

In contrast to the Cu1–O4–Cu2 moiety, the phases of the $\mathbf{E} \parallel ab$ first shell EXAFS over the same temperature range (Fig. 3) are within 0.006 Å of each other, indicating that the RDFs of the Cu2–O2,3 and Cu1–O1 pairs are not dramatically affected by the superconducting transition. Any changes in these spectra and thus any corresponding alterations of the structure in the *ab* direction, for example, breathing modes that could be associated with intraplanar charge transfer (*30*), must be more subtle, from the EXAFS perspective, than those found for the axial O atom. Large-amplitude motions of O2,3 in the *c* direction (*31, 32*) are not necessarily precluded by these data.

Variations in the EXAFS of unoriented $TlBa_2Ca_3Cu_4O_{11}$ associated with its superconducting transition (T_c ~120 K) are also found. As for $YBa_2Cu_3O_7$, the virtual identity of the phases of the Cu-equatorial O

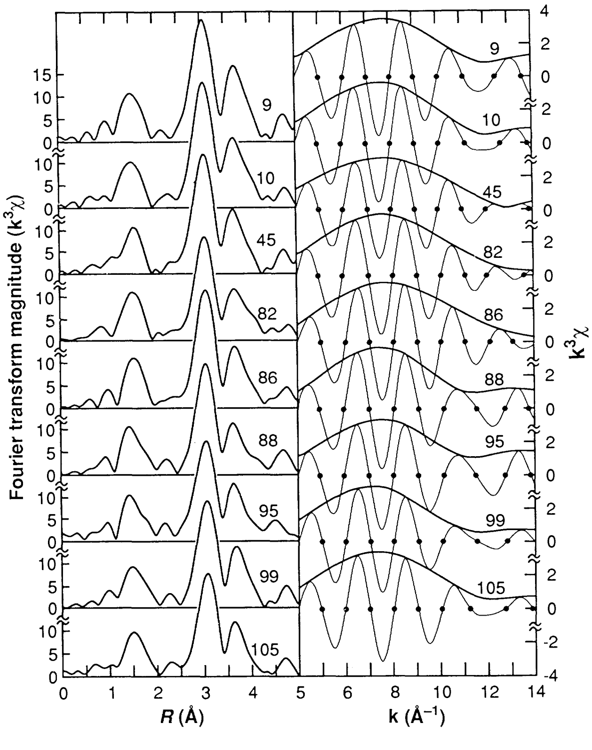

Fig. 2. (**Left**) Fourier transform moduli of the ($\mathbf{k}$ = 4 to 14 Å^{-1}) EXAFS of oriented $YBa_2Cu_3O_7$ $\mathbf{E} \parallel c$ at 9, 10, 45, 82, 86, 88, 95, 99, and 105 K. The (phase-shifted) contribution of the Cu1–O4 (and part of the Cu2–O4) moiety is observed at R = 1.1 to 2.0 Å; the remainder of the Cu2–O4 contribution occurs at R = 1.9 to 2.4 Å. The peaks at higher R represent the contributions of the Y, Ba, and Cu shells. The 9, 86, and 99 K spectra were from one experimental run, the others were measured on a different beam line. (**Right**) Fourier-filtered (back-transformed over approximately R = 1.1 to 2.0 Å) EXAFS (——) and amplitudes (——) of the Cu1–O4 wave, from oriented $YBa_2Cu_3O_7$ $\mathbf{E} \parallel c$, at 9, 10, 45, 82, 86, 88, 95, 99, and 105 K. The nodes (zero-crossings) of the EXAFS, used to identify the behavior of the phase, are depicted by ●. The changes with temperature in the Fourier transform moduli are reflected in the beat at around $\mathbf{k}$ = 12 Å^{-1}. This beat is not present, and the EXAFS is more rapidly damped in the fluctuation region.

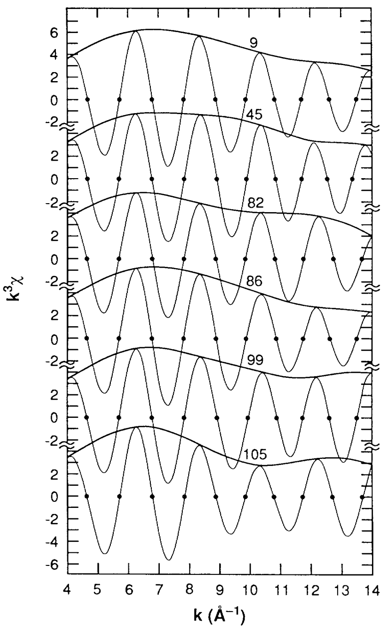

Fig. 3. Fourier-filtered (back-transformed over approximately R = 1.1 to 2.0 Å) EXAFS (——), amplitudes (——), and nodes (●) of the *ab*-oriented Cu–O waves from oriented $YBa_2Cu_3O_7$ E ∥ *ab*, at 9, 45, 82, 86, 99, and 105 K. The absence of any effect on the phase and the small change in amplitude demonstrate that, in contrast to the E ∥ *c* spectra, no substantial changes in the Cu1–O1 or Cu2–2,3 distances, numbers, or MSRDs occur through this temperature range.

waves at all temperatures demonstrates that the average in-plane Cu–O RDF is conserved. For more distant shells (Fig. 4), however, the 2.75 Å peak in the Fourier transform modulus is 25% higher for the superconducting phase, the peak at 2.5 Å has shifted to 2.4 Å and is lower in magnitude and better resolved, and the third peak at 2.2 Å disappears just below T_c and then returns with a unique shape at 10 K. Curve fits show no significant changes in the distances, numbers, or MSRDs for the Ca, Ba, and Cu shells across T_c. We therefore probed the structural perturbation across T_c by computing the difference between the Fourier transform moduli of the Ca-Ba-Cu curve fit and the original data (Fig. 4). On the basis of its position and amplitude, the large peak in these curve-fit residuals at 2 to 2.25 Å corresponds to the contribution of the axial O shell. In shifting from 2.1 Å above T_c to 2.25 Å at T_c and toward $T_{1/2}$ (and subsequently presenting a novel shape at 10 K), this "axial O" peak is the only feature that demonstrates the temperature dependence of the original data. The conclusion that a structural perturbation centered at the axial O accompanies the superconducting transition in $TlBa_2Ca_3Cu_4O_{11}$ is therefore compelling.

On back-transforming these residuals, we find that a beat is observed at **k** = 11 to 13 Å^{-1} for $T > T_c$ but not below T_c. Such behavior would occur if the Cu-O wave became more damped with the superconducting transition, as was observed in the EXAFS of $YBa_2Cu_3O_7$, because of an increase in the MSRD. Although we cannot discern whether the Cu–axial O RDF subsequently reverts to that of the nonsuperconducting phase at low T, it is clear that there is a fluctuation region near T_c in which the structure differs from that at both higher and lower temperatures. This scenario is not only the most plausible interpretation of the EXAFS, it is also similar to the temperature dependence of the axial O in $YBa_2Cu_3O_7$. We therefore believe that all aspects of the lattice instability accompanying the superconducting transition—its existence, the localization of this instability in the axial O atom, its occurrence in a fluctuation region beginning near T_c, and its description as a sudden change in the MSRD of the axial O, which may be due to a double-well structure outside the fluctuation region that softens in the vicinity of T_c—are very similar in $YBa_2Cu_3O_7$ and $TlBa_2Ca_3Cu_4O_{11}$.

In addition to the related phases that can be prepared by, for example, changing the stoichiometries within a class of compounds (*13, 33*) or the non-Cu cations in $YBa_2Cu_3O_7$ (*34*), more subtle modification of the properties of these compounds can also be accomplished by low concentration doping. In this regard we have measured the polarized EXAFS at 10 K of two derivatives of $YBa_2Cu_3O_7$: $YBa_2Cu_3O_{6.5}$ and $YBa_2Cu_{2.8}Co_{0.2}O_{7+\delta}$. The principal structural distortion accompanying the removal of the O1 atoms from the self-doped orthorhombic material (*35*) is a decrease of the Cu1–axial O4 bond lengths (7). Cobalt substitutes specifically for Cu1 and most greatly affects the *c*-lattice parameter (*36*). At the dopant levels used here the alteration of the equatorial Cu–O distance is minimal (*7, 36*). The *ab*-oriented Cu–O waves in these three materials at 10 K are virtually identical in both phase and amplitude (Fig. 5, curve a). The EXAFS from Cu1–O4 below **k** = 10 Å^{-1} is also unaffected, so that the average Cu1–O4 distance, the O4 occupancy, and the harmonic component of the MSRD are conserved (Fig. 5, curve b). However, doping does affect the amplitude above 8 Å^{-1} and the phase in the beat region at 10 to 13 Å^{-1} in a way identical to that induced by temperature within the fluctuation region. Thus, modifications of the atomic and electronic structure that affect the superconductivity also specifically affect the axial O structure in the same way as temperature.

The data we have presented here demonstrate that for the high-temperature superconductors $YBa_2Cu_3O_7$ and $TlBa_2Ca_3Cu_4O_{11}$ a structural perturbation involving a specific local mode, namely, a lattice instability that is localized at the axial O site, occurs around the superconducting transi-

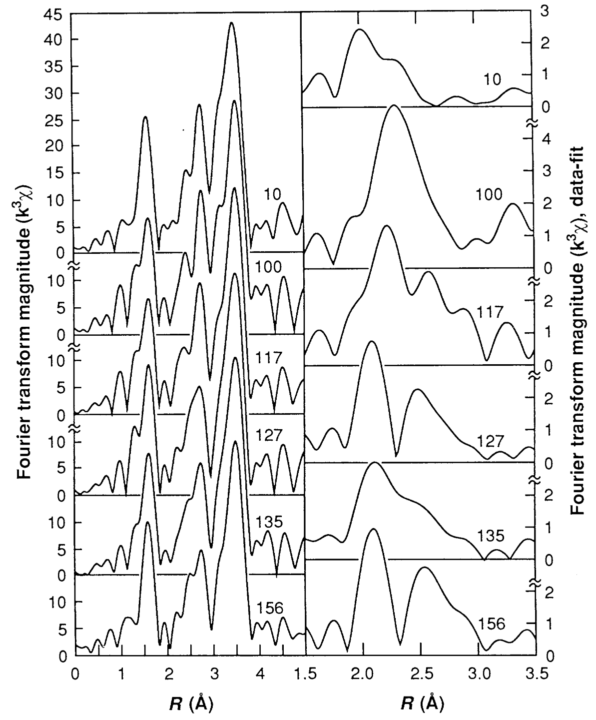

Fig. 4. (**Left**) Fourier transform moduli of the (**k** = 4 to 16 Å^{-1}) EXAFS of (unoriented) $TlBa_2Ca_3Cu_4O_{11}$ at 10, 100, 117, 127, 135, and 156 K. The features in the region R = 2 to 3 Å are very similar for the three spectra above T_c (~120 K) and for the two spectra at 100 and 117 K, but distinct changes in the positions and relative intensities of the peaks in the region of the axial O, Ca, and Ba contributions are observed across the superconducting transition. (**Right**) Fourier transform moduli of the curve-fit residual from the EXAFS of $TlBa_2Ca_3Cu_4O_{11}$ at 10, 100, 117, 127, 135, and 156 K, obtained by subtracting the calculated three-wave, Cu–Ca, Cu–Ba, and Cu–Cu EXAFS from the actual data and then transforming over the range **k** = 4 to 16 Å^{-1}. The primary contribution of the axial O will be within R = 2.0 to 2.5 Å, residuals from the Cu–Ca and Cu–Ba waves should lie at a somewhat higher R. Above T_c, the similarities between the 127 and 156 K data are evident, and the 135 K result is very similar in terms of the positions and relative intensities of the three peaks at 2.1, 2.5, and 2.9 Å. A shift in the position of the main peak to 2.25 to 2.30 Å, as well as other changes, occurs in the higher temperature range of the superconducting phase, followed by a novel, low-magnitude pattern as the temperature is further decreased to 10 K.

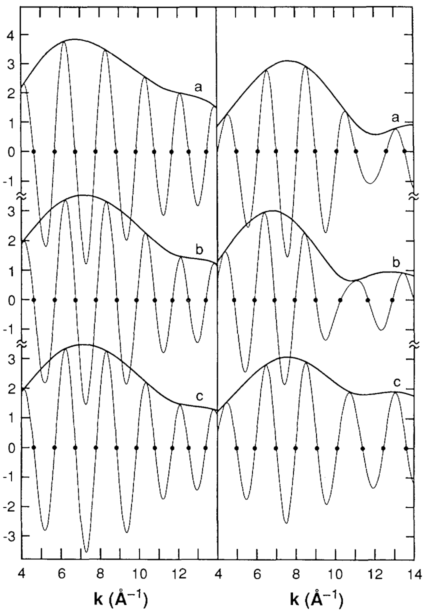

Fig. 5. (**Left**) Fourier-filtered (back-transformed over approximately $R = 1.1$ to 2.0 Å) EXAFS (——), amplitudes (——), and nodes (●) of the Cu1,2–O,1,2,3 wave from **E** ∥ *ab* oriented $YBa_2Cu_3O_7$ (a), $YBa_2Cu_3O_{6.5}$ (b), and $YBa_2Cu_{2.8}Co_{0.2}O_{7+\delta}$ (c). Their virtual identity demonstrates that doping at these levels has little or no effect on the *ab*-oriented Cu–O RDFs. (**Right**) Fourier-filtered EXAFS (——), amplitudes (——), and nodes (●) of the Cu1–O4 wave from **E** ∥ *c* oriented $YBa_2Cu_3O_7$ (a), $YBa_2Cu_3O_{6.5}$ (b), and $YBa_2Cu_{2.8}Co_{0.2}O_{7+\delta}$ (c). These were obtained in the same way as for the **E** ∥ *ab* spectra. Doping significantly alters the beat.

tion in these materials. The axial O in both materials apparently resides in a double-well potential that softens in a fluctuation region around T_c.

The type of potential wells that we believe occur in $YBa_2Cu_3O_7$ and $TlBa_2Ca_3Cu_4O_{11}$ are reminiscent of a paraelectric-ferroelectric phase transition (*37*). Similar structures are well known among ABO_3 perovskites. Although the positions of the atoms of the high-T_c materials undergo a fluctuation rather than a transition, the significance of the structural similarities is that the driving force for these types of phase transitions is the internal dielectric response. In the superconductors the atoms already reside in the "low-temperature" form above T_c, and the fluctuation can affect the electronic degeneracy rather than the crystal symmetry. The analogies between the behavior of ferroelectrics and that of the high-T_c materials suggest that the lattice fluctuation in the latter could be driven by a change in the polarization that accompanies the superconducting transition and that is coupled to the *c*-oriented vibrations of the axial O atom. Furthermore, the absence of a bandgap supports a role for electronic factors as contributors to this lattice instability (*37*).

Within this context, we present a tentative scenario for rationalizing the structural information presented above. We suggest that there is intimate coupling between electron (low-energy charge transfer excitations) and phonon dynamics, particularly in the *c*-direction. Indeed, the highly polarizable O atoms in a near-perovskite structure lead to anharmonic lattice dynamics, for example, by integrating out electronic degrees of freedom as in shell-model approaches (*38, 39*). The typical result is an effective double-well, on-site potential for each ion, frequently parameterized as (*39*)

$$V(u) = -au^2 + bu^4 \qquad (1)$$

where a and b are positive (possibly temperature-dependent) constants, and the two terms represent short-range repulsion and long-range attraction. Here u is the displacement coordinate for an atom (or larger complex) with respect to some undistorted structural phase. Equation 1 yields minima at $u_0 = \pm(a/b)^{1/2}$. Each of these double-well, on-site potentials is coupled via (linear or nonlinear) springs in an extended array. It is typical (*39*) to describe structural phase transitions in this kind of approach by supposing that Eq. 1 is an effective Ginzburg-Landau free energy expansion and that the coefficient a is temperature-dependent and changes sign at some temperature T_0: $-a = -a_0(T_0 - T)$, so that the double well ($T < T_0$) is replaced by a single well for $T > T_0$. A typical mean field description, for instance, replaces bu^4 in Eq. 1 with $b\langle u^2\rangle u^2$, where $\langle u^2\rangle$ denotes a thermal average and $\langle u^2\rangle \propto T$. (For simplicity, we do not distinguish normal coordinates from the Landau order parameter in Eq. 1.)

The transition from single to double well outlined above (*40*) is driven by thermal fluctuations; increasing T leads to increasing fluctuation amplitudes that renormalize the bare double-well potential into a single well for $T > T_0$. We suggest that the same renormalization occurs in our coupled electron-ion problem around the superconducting transition temperature. The renormalization of the double well is then driven only indirectly by temperature but more specifically by the critical superconducting fluctuations that modify the effective ion potential through ion-electron coupling. In this scenario, the purely thermal softening of the double well occurs at $T_0 >> T_c$, so that the double-well structure is expected both above and below T_c. The "critical fluctuation regime," $(T_c - \delta_\ell T) < T < (T_c + \delta_u T)$, is very small in conventional superconductors, but in the present strong-coupling superconductors it is expected to be much larger.

A more graphic description is that superconductivity and this incipient (anti)ferroelectric type of behavior represent alternative, competing phases, both of which are coupled to the same vibronic and electronic channels affecting the motion of the axial O atom. Within the fluctuation region, the effects on these channels of the factors associated with the onset of superconductivity increase the vibrational motion of this ion. At sufficiently large displacements the paraelectric phase becomes favored over the normal (at these temperatures) ferroelectric structure. However, as the fluctuations in these channels condense approaching $T_c - \delta_\ell T$, the superconducting phase settles in and the structure reverts to the original (anti)ferroelectric form.

Mechanistically, we suggest a three-step process by which the *c*-axis polarizability could enhance (or even induce) pairing in the CuO_2 planes. The charge transfer excitations in the *c* direction are the microscopic origin of the polarizability. These act as a nonlinear "pump" driving intrinsically soft phonons in the plane into anharmonic regimes—analogously to a nonlinear dynamic Jahn-Teller mechanism. This in-plane nonlinear electron-phonon activity then synergistically couples to and augments intrinsic in-plane pairing mechanisms (spin fluctuations and charge transfer).

It is expected (*12, 41*) that strongly anharmonic axial O motions will modify Cu orbitals in the plane and drive large-amplitude (anharmonic) Jahn-Teller or buckling modes (*32*) of the plane octahedra. We have demonstrated (*12, 41*) that charge transfer coupled to appropriate lattice dynamics can explain the anomalously large oscillator strength of an infrared-active phonon mode observed (*11*) in superconducting $YBa_2Cu_3O_7$ at ~155 cm^{-1}; this normal mode is well described as a rigid motion of CuO_3 clusters (Cu–O chain plus two O4 oxygens) in the *c* direction with counter-motion of the Ba^{2+} ions. A corresponding symmetric (Raman-active) mode in the *c* direction is also predicted and observed (*13*). In addition, large *c*-axis dielectric constants have been observed in $YBa_2Cu_3O_7$ (*32, 42*) and interpreted as being the result of the close proximity of a true (anti)ferroelectric distortion in this direction with large amplitude O displacements (*43*).

The above scenario should not be confused either with simple charge fluctuation pairing or with harmonic electron-phonon Bardeen-Cooper-Schrieffer theory. Rather, the large amplitude phonon modes in the plane are driven into nonthermal regimes by the local charge-transfer "pump," relying on specific structural and chemical features.

We conclude with three important remarks. First, previous experimental evidence for *c*-axis charge transfer and phonon coupling has focused on effects of doping [for example, O content in $YBa_2Cu_3O_{7-\delta}$ (*7*, *41*)]. Our present data suggest similar activity as a function of temperature in the superconducting onset regime. Second, the large fluctuation regime and variations of effective ion potential that we have suggested around T_c should be reflected in ion and electron dynamics, as in conventional perovskite transitions. Thus, elastic constants, inelastic neutron scattering, nuclear magnetic resonance, and electron paramagnetic resonance, both in the plane and in the *c* direction, can be expected to become increasingly important probes to discriminate time scales (*39*). For instance, central peak scattering from domain motion and *c*-direction sound speed anomalies can be anticipated. Third, complete analysis of EXAFS data in the strong anharmonic situations envisaged demands extensions of harmonic Debye-Waller factor theory (*17*). Ab initio analysis of our EXAFS data is in progress (*29*).

Note added in proof: Results from (*29*) indicate that the effective potential for the Cu1–O4 relative motion is a deep double well that is present at all studied temperatures, and the motion of the O4 atom is best described in a quantum mechanical regime. In the fluctuation region the minima of the potential move closer to each other, decreasing the separation in distance and the height of the potential barrier between the two minima of the potential.

REFERENCES AND NOTES

1. J. G. Bednorz and K. A. Müller, *Z. Phys. B* **64**, 189 (1986); M. K. Wu *et al.*, *Phys. Rev. Lett.* **58**, 908 (1987); H. Maeda, Y. Tanaka, M. Fukutomi, T. Asano, *Jpn. J. Appl. Phys.* **27**, L209 (1988); Z. Z. Sheng and A. M. Hermann, *Nature* **332**, 55 (1988); Y. Tokura *et al.*, *ibid.* **337**, 345 (1989).
2. See, for example, T. M. Rice, *Z. Phys. B* **67**, 141 (1987); W. A. Little, *Science* **242**, 1390 (1988); K. A. Müller, *Proceedings of the Workshop on High Temperature Superconductors* (Oberlech, Austria, August 1988) (IBM Research Journal, Zurich, 1989).
3. W. L. McMillan, *Phys. Rev.* **167**, 331 (1968).
4. R. J. Cava *et al.*, *Nature* **332**, 814 (1988).
5. J. F. Zasadzinski *et al.*, *Physica C* **158**, 519 (1989); C.-K. Loong *et al.*, *Phys. Rev. Lett.* **62**, 2628 (1989); P. B. Allen, *Nature* **339**, 428 (1989).
6. A. R. Bishop *et al.*, *Z. Phys. B* **76**, 17 (1989).
7. R. J. Cava *et al.*, *Physica B* **153–155**, 560 (1988).
8. M. Mali *et al.*, *Phys. Lett. A* **124**, 112 (1987); N. Nücker *et al.*, *Phys. Rev. B* **37**, 5158 (1988); A. Bianconi *et al.*, *ibid.* **38**, 7196 (1988); C. Taliani *et al.*, *Solid State Commun.* **66**, 487 (1988).
9. S. D. Conradson and I. D. Raistrick, *Science* **243**, 1340 (1989); H. Maruyama *et al.*, *Physica C* **160**, 524 (1989).
10. F. Seidler *et al.*, *Physica C* **157**, 375 (1989).
11. L. Genzel *et al.*, *Phys. Rev. B* **40**, 2170 (1989).
12. I. Batistic *et al.*, *ibid.*, p. 6896.
13. R. Zamboni, G. Ruani, A. J. Pal, C. Taliani, *Solid State Commun.* **70**, 813 (1989).
14. R. S. Markiewicz and B. C. Giessen, *Mod. Phys. Lett. B* **3**, 723 (1989); L. Pietronero and S. Strässler, *Phys. Rev. Lett.* **47**, 593 (1981).
15. C. Murayama *et al.*, *Nature* **339**, 293 (1989).
16. J. J. Caponi *et al.*, *Europhys. Lett.* **3**, 1301 (1987); M. A. Beno *et al.*, *Appl. Phys. Lett.* **51**, 57 (1987); W. I. F. David *et al.*, *Nature* **327**, 227 (1987); T. Siegrist *et al.*, *Phys. Rev. B* **35**, 7137 (1987); A. Williams *et al.*, *ibid.* **37**, 7960 (1988).
17. See J. A. Krumhansl, in *Proceedings in Life Sciences: Protein Structure, Molecular and Electronic Reactivity*, R. Austin *et al.*, Eds. (Springer-Verlag, New York, 1987).
18. C. C. Torardi *et al.*, *Science* **240**, 631 (1988).
19. M. A. Subramanian *et al.*, *J. Solid State Chem.* **77**, 192 (1988).
20. P. A. Lee *et al.*, *Rev. Mod. Phys.* **53**, 769 (1981); B.-K. Teo, *EXAFS: Basic Principles and Data Analysis* (Springer-Verlag, New York, 1986).
21. C. Y. Yang *et al.*, *Phys. Rev. B* **38**, 6568 (1988).
22. E. A. Stern and S. M. Heald, in *Handbook on Synchrotron Radiation*, E. E. Koch, Ed. (North-Holland, Amsterdam, 1983), p. 955; S. M. Heald *et al.*, *Phys. Rev. B* **38**, 761 (1988).
23. D. E. Farrell *et al.*, *Phys. Rev. B* **36**, 4025 (1987).
24. I. Ihara *et al.*, *Nature* **334**, 510 (1988); H. Ihara *et al.*, *Phys. Rev. B* **38**, 11952 (1988).
25. B.-K. Teo, *J. Am. Chem. Soc.* **103**, 3990 (1981); J. J. Bolan *et al.*, *J. Chem. Phys.* **77**, 142 (1982).
26. S. P. Cramer, K. O. Hodgson, E. I. Steifel, W. E. Newton, *J. Am. Chem. Soc.* **100**, 2748 (1978).
27. P. Eisenberger and G. S. Brown, *Solid State Commun.* **29**, 481 (1979); E. D. Crozier and A. J. Seary, *Can. J. Phys.* **58**, 1388 (1980); P. Eisenberger and B. Lengeler, *Phys. Rev. B* **22**, 3551 (1980); C. Bouldin and E. A. Stern, *ibid.* **25**, 3462 (1982).
28. S. D. Conradson and I. D. Raistrick, unpublished data.
29. J. Mustre de Leon, S. D. Conradson, I. Batistic, A. R. Bishop, manuscripts in preparation. Curve fits based on a novel approach, calculations of the EXAFS from a particular potential function floating the parameters which determine the potential to optimize the fit, provide direct support for this model of the structure and its temperature dependence beyond the qualitative analysis given here.
30. B. Renker *et al.*, *Z. Phys. B* **67**, 15 (1987).
31. D. Reagor *et al.*, *Phys. Rev. Lett.* **62**, 2048 (1989).
32. H. Monien and A. Zawadowski, *Phys. Rev. B* **41**, 6297 (1990).
33. M. Hervieu *et al.*, *J. Solid State Chem.* **75**, 212 (1988); J. B. Parise *et al.*, *ibid.* **76**, 432 (1988).
34. R. J. Cava *et al.*, *Nature* **336**, 211 (1988).
35. A. Santoro *et al.*, *Mater. Res. Bull.* **22**, 1007 (1987); S. Katano *et al.*, *Jpn. J. Appl. Phys.* **26**, L1049 (1987); R. J. Cava *et al.*, *Phys. Rev. B* **36**, 5719 (1987).
36. D. Shindo *et al.*, *Jpn. J. Appl. Phys.* **26**, L1667 (1987); J. M. Tarascon *et al.*, *Phys. Rev. B* **37**, 7458 (1988); T. J. Kistenmacher, *ibid.* **38**, 8862 (1988).
37. M. E. Lines and A. M. Glass, *Principles and Applications of Ferroelectrics and Related Materials* (Clarendon, Oxford, 1977).
38. S. K. Kurtz *et al.*, *Ferroelectrics* **87**, 29 (1988); A. Bussman-Holder *et al.*, *Phys. Rev. B* **39**, 207 (1989).
39. A. D. Bruce and R. A. Cowley, *Adv. Phys.* **29**, 219 (1980).
40. It is important to realize that the static potential double-well description we have given may only be a convenient parameterization. As in other structurally transforming perovskites (*39*), the true situation may very well be dynamic but with slower reorientation time scales, associated, for instance, with domain motions: such time scales may be strongly renormalized to lower frequencies in the transition region and below. EXAFS is effectively instantaneous (10^{-15} s) and therefore gives information of only "frozen" snapshot profiles. Alternative techniques are needed to discriminate the various possible time scales (*39*).
41. Z. Tesanovic, A. R. Bishop, R. L. Martin, *Solid State Commun.* **68**, 337 (1988).
42. L. R. Testardi, W. G. Moulton, H. Mathias, H. K. Ng, C. M. Rey, *Phys. Rev. B* **37**, 2324 (1988).
43. S. K. Kurtz *et al.*, *Mater. Lett.* **6**, 317 (1989).
44. We thank A. Mayer, T. Rollet, and R. Sherman for sample preparation and x-ray powder diffraction analysis; J. Thompson for performing magnetic susceptibility measurements; J. Beery for the conductivity measurements; M. Aronson, F. Garzon, and the SSRL operations staff for their assistance in acquiring these data; R. Albers, R. Martin, Z. Fisk, D. Smith, J. Smith, K. Müller, and D. Reagor for useful discussions and for reviewing this manuscript; and R. Scott for the XAFPAK data analysis software. Data acquisition and some analysis were done at SSRL, which is funded by the Department of Energy under contract DE-AC03-82ER-13000, Office of Basic Energy Sciences, Division of Chemical Sciences and the National Institute of Health Biotechnology Resource Program, Division of Research Resources. This work was supported by the Department of Energy.

25 July 1989; accepted 27 February 1990

North-South Contraction of the Mojave Block and Strike-Slip Tectonics in Southern California

J. M. Bartley, A. F. Glazner, E. R. Schermer

The Mojave block of southern California has undergone significant late Cenozoic north-south contraction. This previously unappreciated deformation may account for part of the discrepancy between neotectonic and plate-tectonic estimates of Pacific–North American plate motion, and for part of the Big Bend in the San Andreas fault. In the eastern Mojave block, contraction is superimposed on early Miocene crustal extension. In the western Mojave block, contractional folds and reverse faults have been mistaken for extensional structures. The three-dimensional complexity of the contractional structures may mean that rigid-block tectonic models of the region based primarily on paleomagnetic data are unreliable.

Deformation of the Mojave block of southern California (Fig. 1) is linked to such diverse neotectonic phenomena as movement on the San Andreas and Garlock faults, thrust faulting in the Transverse Ranges, rotation of crustal blocks, and development of the Big Bend in the San Andreas fault (*1*–*4*). The importance of these features to tectonic and seismic-hazard studies makes it vital to determine the kinematics of deformation in the Mojave block.

J. M. Bartley, Department of Geology and Geophysics, University of Utah, Salt Lake City, UT 84112.
A. F. Glazner, Department of Geology, Campus Box 3315, University of North Carolina, Chapel Hill, NC 27599.
E. R. Schermer, Department of Geological Sciences, University of California, Santa Barbara, CA 93106.